ANNALS OF GEOPHYSICS, 68, 3, NS338, 2025; doi:10.4401/ag-9240
OPEN ACCESS

Seismic structure at the test site for wind energy research, WINSENT, Southwest Germany

Jan R. Hirsch[1], Joachim R. R. Ritter[*,1]

(1) Karlsruhe Institute of Technology, Geophysical Institute, Karlsruhe, Germany

Article history: received January 2, 2025; accepted June 18, 2025

Abstract

The subsurface at the Wind Science and Engineering Test Site in Complex Terrain (WINSENT) in SW Germany is studied to derive its underground structure and 3-D seismic velocity distribution. These parameters are important for further geotechnical studies to better understand the soil-structure interaction of wind turbines and their underground. This knowledge is needed for the save construction of modern wind turbines on land whose nacelles reach altitudes of more than 150 m above the ground. Another issue are ground motions which are emitted from wind turbines and can be measured up to distances of several kilometers. We describe the fieldwork at the wind energy test site and the seismic inversion models. The seismic velocities are low compared to other studies due to the weathering and karstification of the Jurassic limestone at the site. We derive 3-D compressional and shear wave velocity models with minor lateral variation which can be used as input for numerical modelling of wave propagation to explore vibrating wind turbines and their emissions.

Keywords: Shallow seismics; Site characterization; Seismic velocity; Wind turbine noise

1. Introduction

The transition to green or CO_2-free energy is an important step to stop global warming and preserve a habitable planet Earth for future generations. One important way to produce nearly CO_2-free electric power at significant rates is wind energy (International Energy Agency, 2024). Thus, wind turbines (WTs) are erected in large numbers, e.g. in China, US or Germany. In some instances, the installation of WTs causes conflicts with other technologies such as flight monitoring or sensitive measurements (Starreveld, 2023). The latter can be high-precision physics experiments or seismological recording stations (Saccorrotti et al., 2011; Stammler and Ceranna, 2016). Therefore, it is important to understand the excitation mechanisms of ground motion by WTs (Nagel et al., 2021) and the radiation of these seismic waves, in order to design counter measurements or find appropriate protection radii (Lerbs et al., 2020; Limberger et al., 2022).

Moreover, there are too many unknown parameters to fully describe the soil-structure interaction of the geological subsurface and WTs. Only few experiments were undertaken directly at WTs and often local geotechnical data are unknown (Neuffer et al., 2021). A world-wide unique exception is the Wind Science and Engineering Test Site in Complex Terrain, short WINSENT in Southwest Germany (Fig. 1) (https://www.zsw-bw.de/en/research/wind-energy/topics/research-test-site-winsent.html). WINSENT consists of two 0.75 MW WTs along with a massive

instrumentation for scientific measurements. The latter includes four 100 m high masts with meteorological sensors, a bird radar and high-speed cameras for bird monitoring, and geotechnical equipment for measuring soil-structure interaction. Each WT foundation has six 1.4 m deep manholes for geotechnical and geophysical monitoring. Inside these manholes, seismic sensors can be placed in the foundation and there are monitoring systems for soil pressure underneath the foundation and displacement sensors (extensometers) which reach 3.5 m (three ones) and 6.5 m (another three ones) below the foundation (Pena et al., 2025). Hence the induced pressure and movement of the foundation directly at the soil-structure interface can be measured in a world-wide unique experiment at the two WT of the WINSENT test site. In addition, three shallow boreholes with broadband seismic sensors at 6 m depth were installed at WINSENT and temporary seismic experiments are conducted to measure the propagation of seismic waves or ground motions. For these studies, it is important to have a model of the underground at WINSENT which characterizes the local compressional (P) and shear (S) wave velocities (*vp*, *vs*) with depth and their lateral variations. These velocity models represent the Green's functions of the wave propagation and are necessary to invert e.g. for the source time function(s) of the ground motion emissions. The velocity models can be also used as starting models for upcoming inversions using a recent large-N experiment around WINSENT.

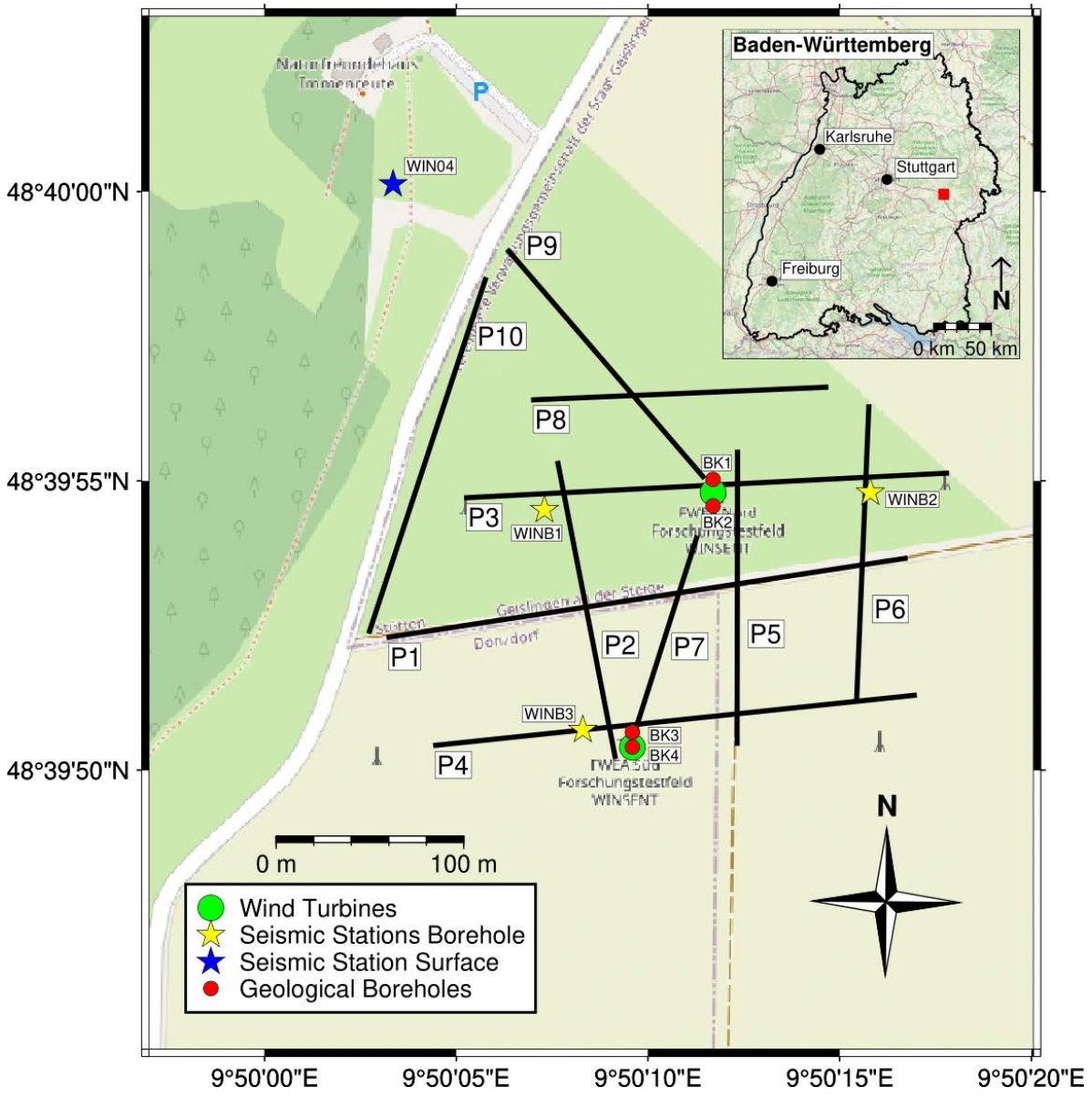

Figure 1. Overview on the WINSENT site and the ten seismic lines (P1-P10). BK1-BK4 are boreholes with geological profiles. The small map shows the position of WINSENT in the state of Baden-Württemberg, SW Germany. Map data from OpenStreetMap.

In the following we describe a shallow seismic refraction experiment at WINSENT. The P- and S-wave data are inverted along ten profiles and the seismic P- and S-wave velocity models are compared with geological profiles at the excavation sites of the foundations and four drill sites. Petrophysical data are also used for comparison with the seismic models and the implications of the results are discussed with respect to ongoing and future geoscientific studies at WINSENT and general geotechnical aspects.

2. Geological background and experimental setting

In this section we will provide an overview of the local geology, a priori information and the seismic experiment.

2.1 Geological setting

WINSENT is especially designed to study different aspects of wind energy harvesting in regions with pronounced topography. Such a mountainous terrain has specific wind flow patterns and weather situations which are different from lowland situations along coastal regions. Also, the underground is often different to the widespread Quaternary sediments in lowlands. Thus, WINSENT is built close to the escarpment of the Swabian Alb, a mountainous region in Southwest Germany. The steep escarpment ('Albtrauf') is about 160 m high and WINSENT is built ca. 150 m west of it on a peneplain composed of limestone of Middle and Upper Jurassic age. The foundations of the WTs are built on white Kimmeridgium limestone (locally named 'Untere Felsenkalkformation') (Regierungspräsidium Freiburg, Landesamt für Geologie, Rohstoffe und Bergbau, 2021) with a thin cover of soil and clay (5-20 cm). A nearly horizontal layering of the limestone layers is expected and in places there is karstification with clay-filled cavities (Fig. 2). WINSENT is thus ideal to study soil-structure interaction at a site with stiff underground and the propagation of emitted ground motions in hard rock and complex topography which may cause amplitude amplification effects (Limberger et al., 2022; Gaßner et al., 2023).

Figure 2. Excavation for the foundation of the southern WT. A thin cover of soil ('Braunerde') is on top of the Jurassic limestone ('Untere Felsenkalkformation, joFU'). The limestone has a weathering zone of varying thickness and karstification with clay fillings. © J. Ritter, KIT-GPI.

2.2 Seismic measurements

Fieldwork for data acquisition was done in May and June 2024. The aim of the measurements was to achieve ca. 20 m deep reaching models of P- and S-wave velocities. To reach this depth, seismic arrivals along ca. 200 m long lines need to be recorded. Our original plan was to use a small explosive source, SISSY – Seismic Impulse Source System (GEOSYM, 2024). However, this could not be put into practice, because we were not able to drill by hand deep enough (ca. 80 cm) into the limestone and using a small drilling rig would have been to elaborate. Therefore,

traditional hammer blows by hand had to be used as source. The latter have a lower source strength and therefore the P-wave arrivals had low amplitudes. Another drawback was a stronger excitation of surface waves due to hammer blows which can mask body wave arrivals at short distances (first ca. 10 m). P-waves were generated with vertical blows on a metal disc, S-waves were excited by hitting on a tripod steel frame perpendicular to the geophone line what might be more effective than explosions for the S-wave excitation. Eight blows with a 5-kg hammer were stacked at each shot point to increase the signal-to-noise ratio (SNR). The average shot point distance was 20 m.

Data acquisition was mostly done with 72 vertical geophones (4.5 Hz natural frequency) placed at 2 m distance along a 142 m long line (incl. 2 m distance from the first shot point). The sensors were connected to three GEOMETRICS Geode recorders with 24 channels (GEOMETRICS, 2024). For the longer lines P1, P2 and P4, two GEODE recorders were moved from the starting point of the line to its end; this allowed the recording for another 96 m (Fig. 3). The sampling rate was set at 8000 samples per second (or $\Delta t = 0.125$ ms). In order to clearly identify the wave type (P or S) in the seismogram sections and the seismic phases at short distances, experiments with short geophone distances and 3-D geophones were conducted along profile P10. In the field, the quality of the waveforms was briefly checked after each hammer blow with a laptop. After fieldwork, the data was converted to the SEG-Y format and 248 datasets for the different shot points were archived.

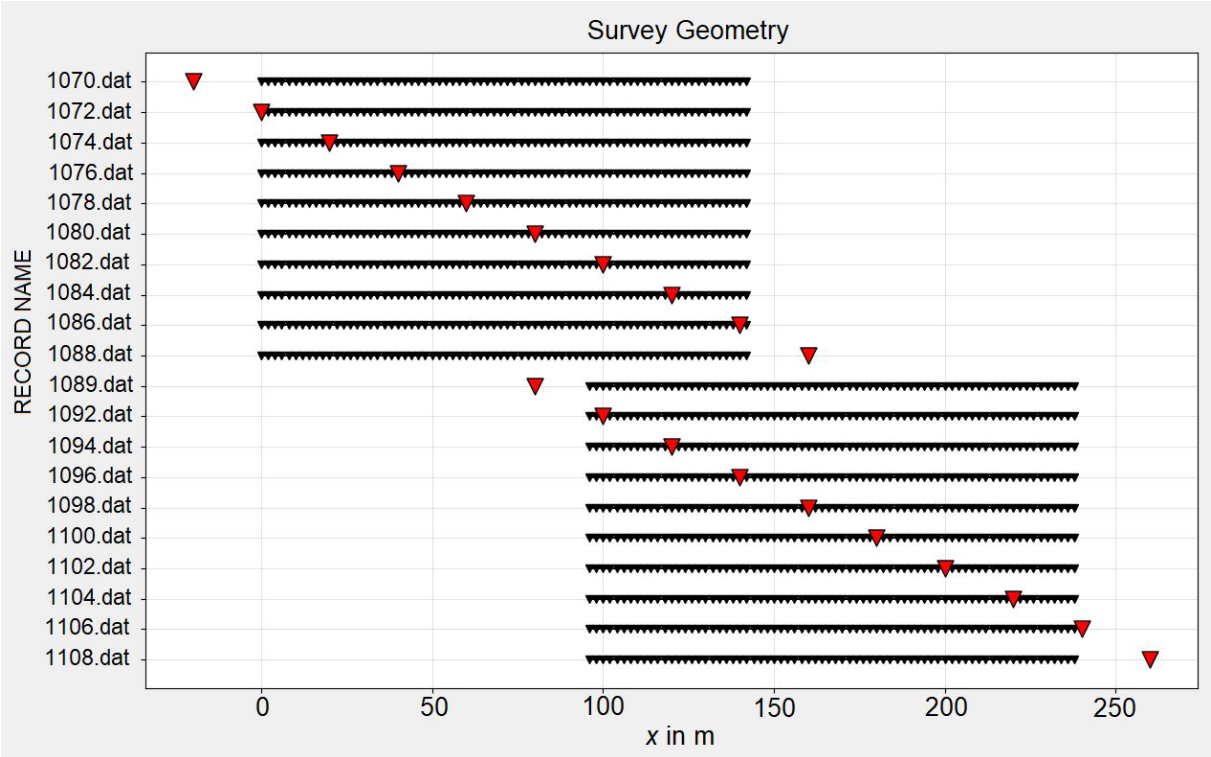

Figure 3. Acquisition geometry: shot points (inverted red triangles) were placed at 20 m distances. To increase the length of the lines, at their ends additional shots were done. 72 geophones (black) had 2 m distance and were grouped with three 24-channel GEODE recorders. After recording of the left part of the line with 10 shot points, the first 48 geophones were place at the end of the line for another 10 shot points. For each shot recording a separate datafile (*.doc) was recorded.

3. Data analysis

3.1 Seismic phase identification and picking

Data examples are given in Figs. 4 and 5 as seismogram sections. Due to the remote location the noise level was low and recording was interrupted when traffic passed by on a neighboring road. The main noise source was the air wave produced of the hammer blows (Fig. 4a) whose amplitudes clearly exceed the seismic wave amplitudes.

The air wave can be identified by the typical constant apparent velocity of 343-344 m/s at frequencies higher than about 100 Hz. In order to suppress such air wave signals we filtered the recordings with a bandpass of 10-100 Hz to enhance the seismic signals.

Clear first arrivals of seismic P-waves can be identified as far as 200 m. The identification of the seismic P- and S-wave phases required some tests with 3-D geophone recording and variations of geophone distances. Our standard recording procedure with 2 m geophone distance and only vertical recording – to save recording channels and work time – fails to recover the seismic phases, especially at distances of less than 10 m. The waves in the thin soil cover and weathering layer (<0.2-0.5 m, see Fig. 2) cannot be identified at 2 m distances and wrong phase identifications could result with misleading phase velocities. To clearly detect and assign arrivals of seismic phases from shallow structures or layers, we reduced the geophone distances to 0.5 m and 1.0 m at <5 m and <10 m shot point distance, respectively, along line P10. In addition, we deployed horizontal geophones at short distances in order to better identify S-wave arrivals in the record sections (note horizontal wave excitation was done along all lines).

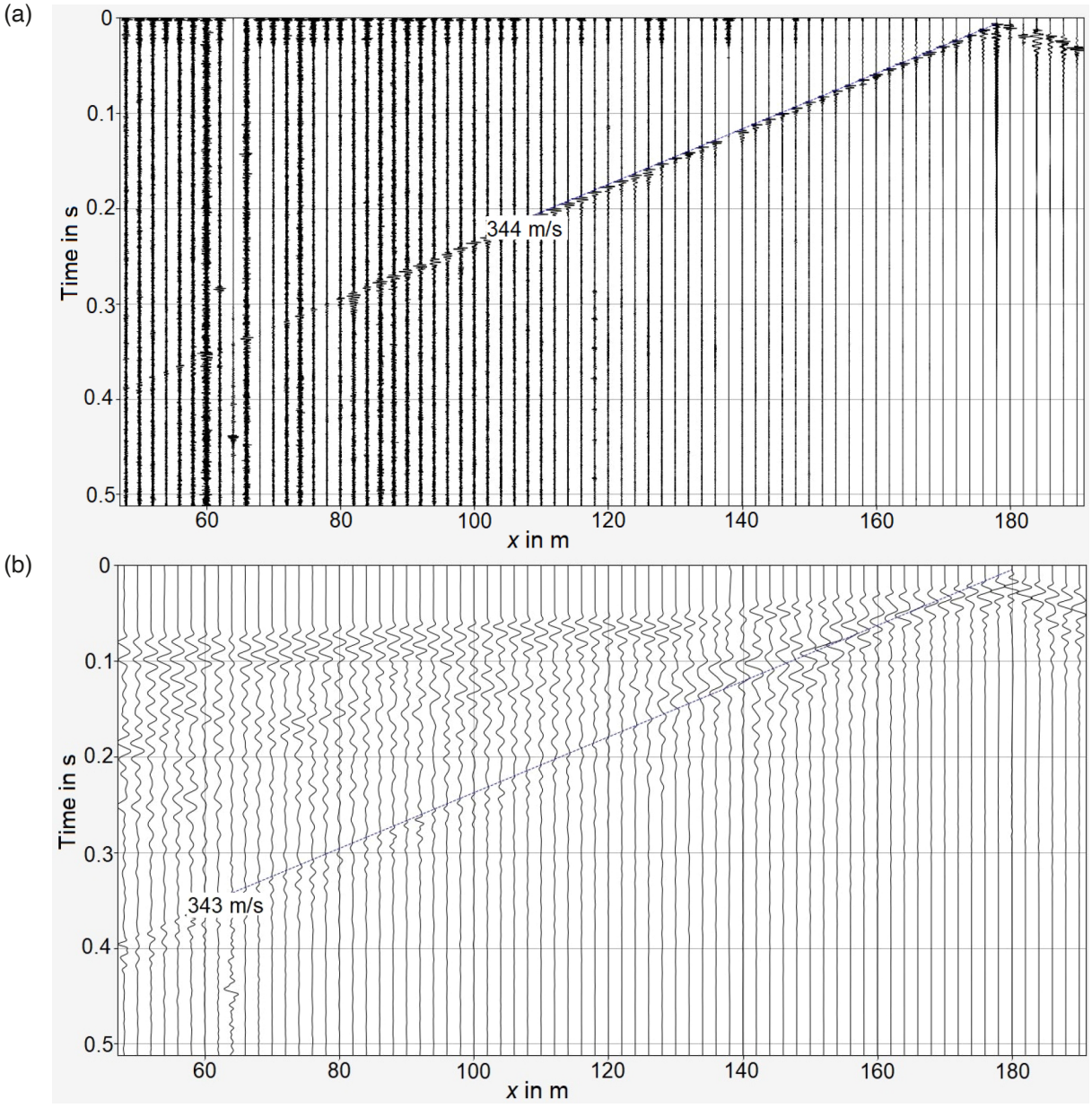

Figure 4. (a) Seismic record sections at high frequencies (>500 Hz), (b) at low frequencies (<100 Hz). Note the difference of the appearance of the air wave with 344 m/s and 343 m/s apparent propagation velocities due to the hammer blow. The source is at distance (*x*) 180 m along the line.

In Fig. 5a there are three visible branches with first arrivals from P-wave phases with apparent propagation velocities of 500 m/s, 1,700 m/s and 3,100 m/s along line P10. The S-waves on the transverse recording component, which are also propagating in three possible layers (Fig. 5b), have apparent velocities of 160 m/s, 800 m/s and 1,600 m/s along the same line P10 (Fig. 1). The *vp*/*vs* ratios for these phases are 3.13, 2.13 and 1.94 what is quite reasonable for shallow layers with partly loose rocks embedded in soil and clay (Fig. 2). The increase of *vp*/*vs* with depth can be explained with pressure-related compaction of the medium. Ground water does not play a role for the observed seismic phases, because the ground water level is much deeper than our wave penetration due to the karstification of the limestone.

The data and apparent velocities of the other lines are quite similar. The phase picking of first arrivals was finally done with *Refrapick*, a routine in the software package *Refrapy* (Guedes et al., 2022). *Refrapy* is an open-source software package which is freely available through GitHub (https://github.com/viictorjs/Refrapy, last access 30. Dec. 2024). It allows to plot, filter and pick the phase arrivals as well as store the pick times for a travel time inversion and model building. Repeated picking finds a picking precision of about ±5 ms for both, the P- and S-wave phases.

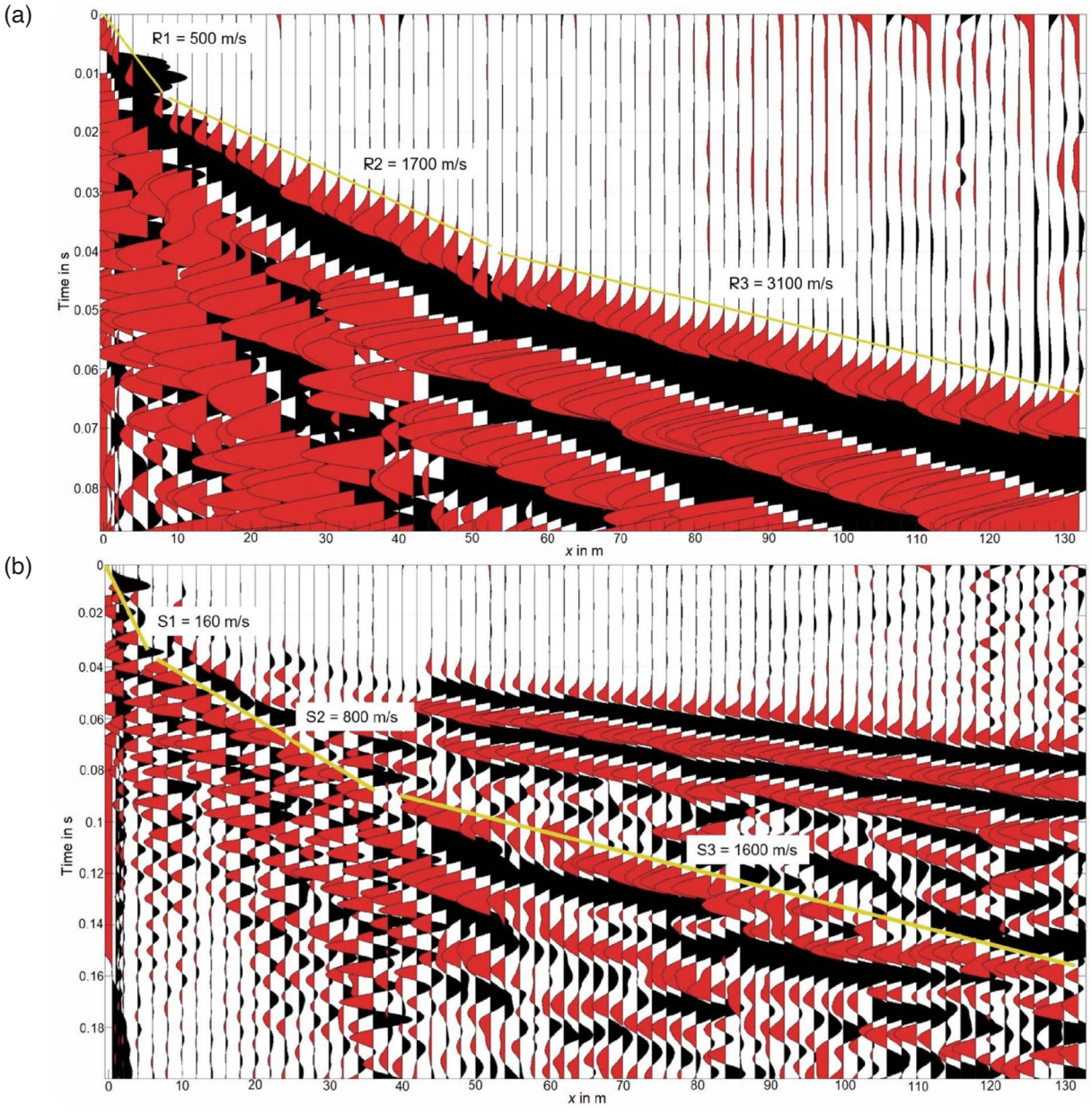

Figure 5. (a) Seismogram section with three identified P-wave phases (R1, R2 and R3) and their apparent velocities along line P10. The vertical component recordings are bandpass filtered from 10 Hz to 100 Hz, *x* is lateral distance along the line. (b) Correspondingly identified S-wave phases (S1, S2 and S3).

3.2 Inversion and seismic velocity models

Seismic velocities are determined by inversion of the first-arrival travel times using the package *Refrainv*, another part of *Refrapy* (Guedes et al., 2022). The linear inverse calculation is done with an iterative approach to account for non-linearities and the maximum number of iterations is set to 20. We use a smoothing parameter $\lambda = 100$ for minimization of the cost function during the inversion and a vertical-to-horizontal smoothing operator of 0.2 to enhance lateral layering but keeping a good vertical resolution (Guedes et al., 2022). The mesh for the model parameters has a discretization of 6 m and the relative distance for refinement nodes of a cell was 0.33 cell dimensions (or 3 nodes per cell). This parameterization cannot resolve soil stratigraphy; however, the soil cover is very thin (5-20 cm) at the WINSENT test site (Fig. 2).

The *vp* data fit for line P8 is given in Fig. 6. This comparison of the observed and picked travel time arrivals with the model-predicted arrivals has a very good coincidence with differences mostly below 0.005 s, the picking uncertainty. The relative root mean square (RMS) is 11.54% in this case what also indicates that the model can well explain the observations. Similar fitting qualities are achieved also for the other lines with relative RMS values of 8.97% to 12.78%.

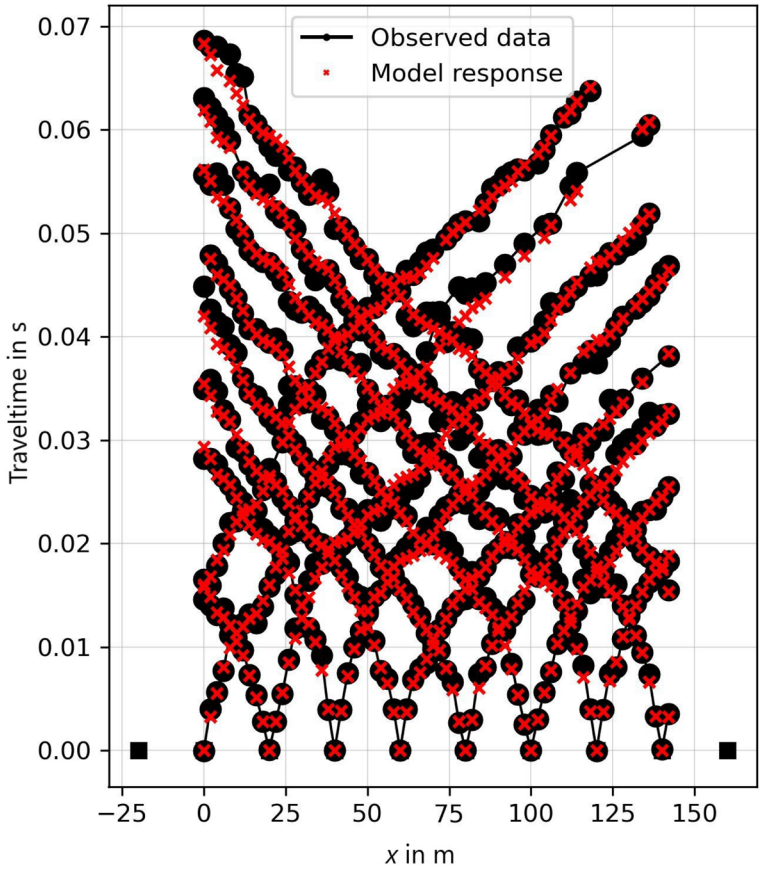

Figure 6. Comparison of observed (black) and modelled (red) P-wave travel times along line P8 with 8 shot points, *x* is lateral distance. The relative root mean square of this fit is 11.54% after 20 iterations and the average time difference is about 0.005 s what corresponds to the reading uncertainty.

In Fig. 7 results for the P-wave and S-wave velocity modelling are presented for the ten lines. Both, P- and S-wave models, contain a strong vertical velocity gradient. Below the thin soil layer, the upper ca. 2 m depth are characterized by low *vp* of about 1,000-1,500 m/s and low *vs* of about 500-800 m/s. Along some lines (P1, P3, P4, P6 and P8) an undulated structure appears in the upper 2 m which is not due to the subsurface, but the acquisition geometry. Here, the low-velocity areas coincide with the shot points; hence the better ray coverage can image the depth range of the near-surface low velocity close to the shot points. In between the shot points, the modeling interpolates the deeper and higher seismic velocity upwards to the surface. Down to ca. 10 m depth, *vp* is in the

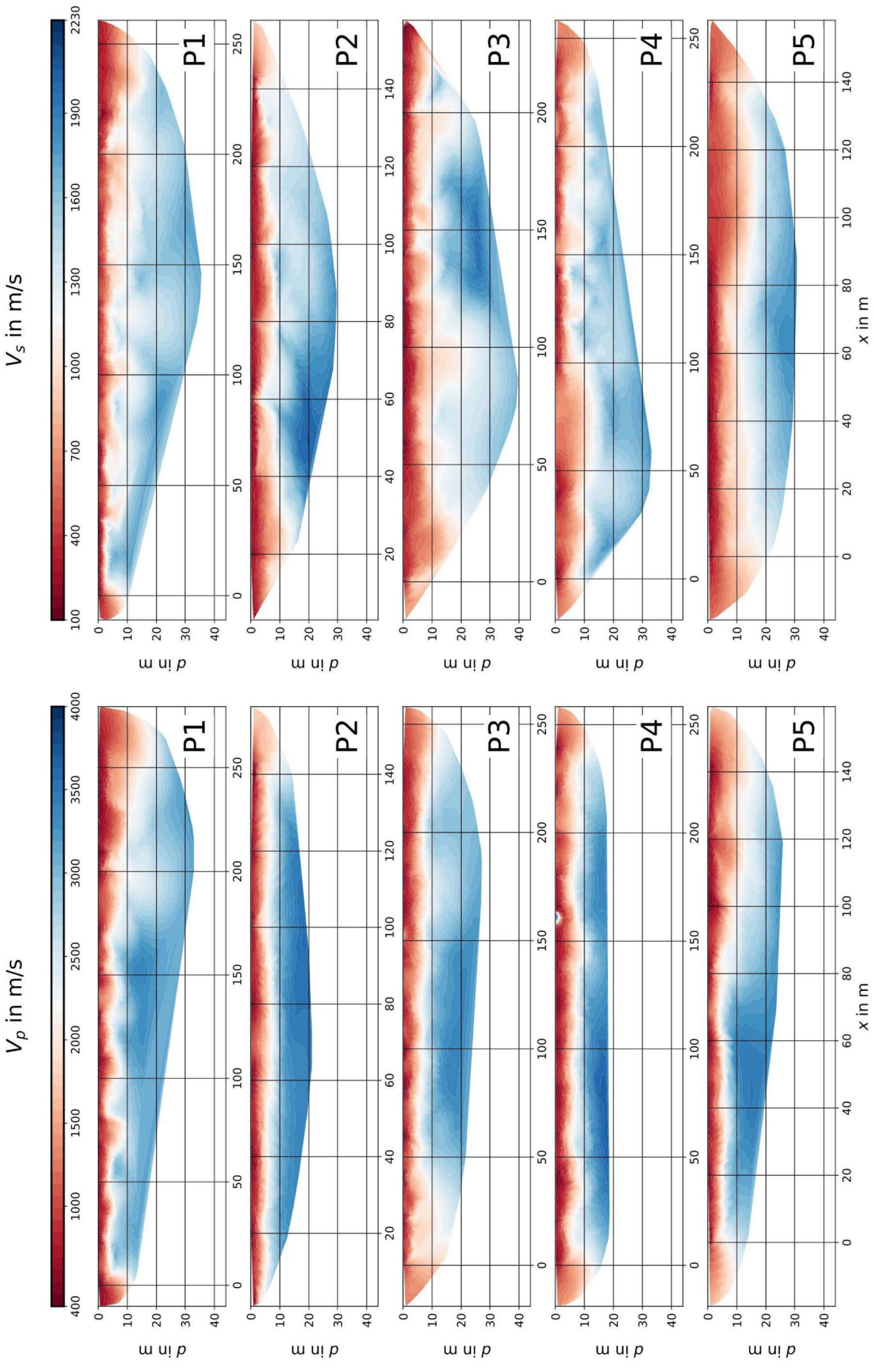
V_p in m/s
V_s in m/s
P1
P2
P3
P4
P5
d in m
x in m

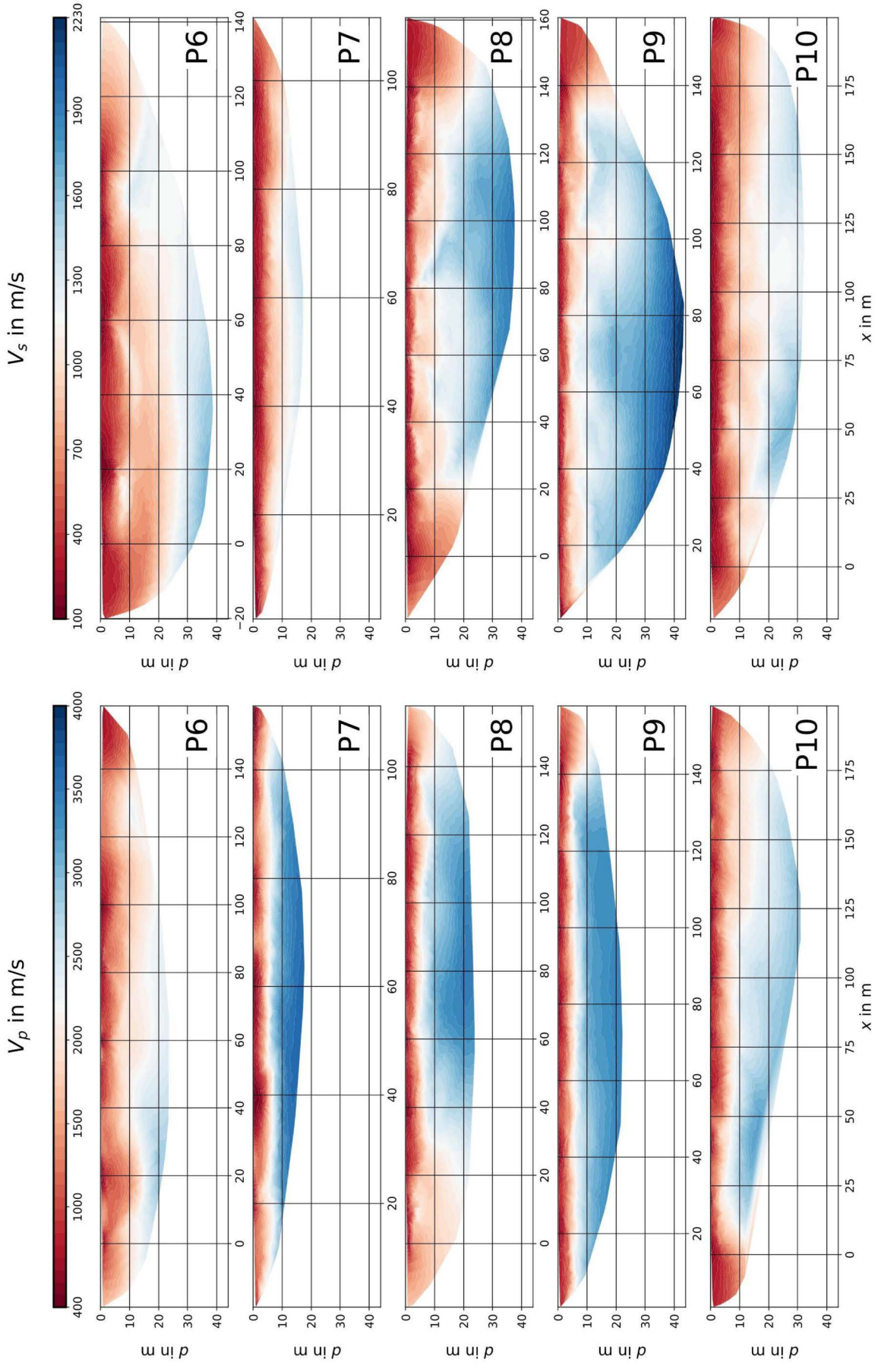

Figure 7. Final seismic velocity models (left: *vp*; right: *vs*) after iterative inversion, *d* is depth. Areas with no ray coverage are faded out. P1-P10 are the lines in the map in Fig. 1. Note that lateral distance is varying.

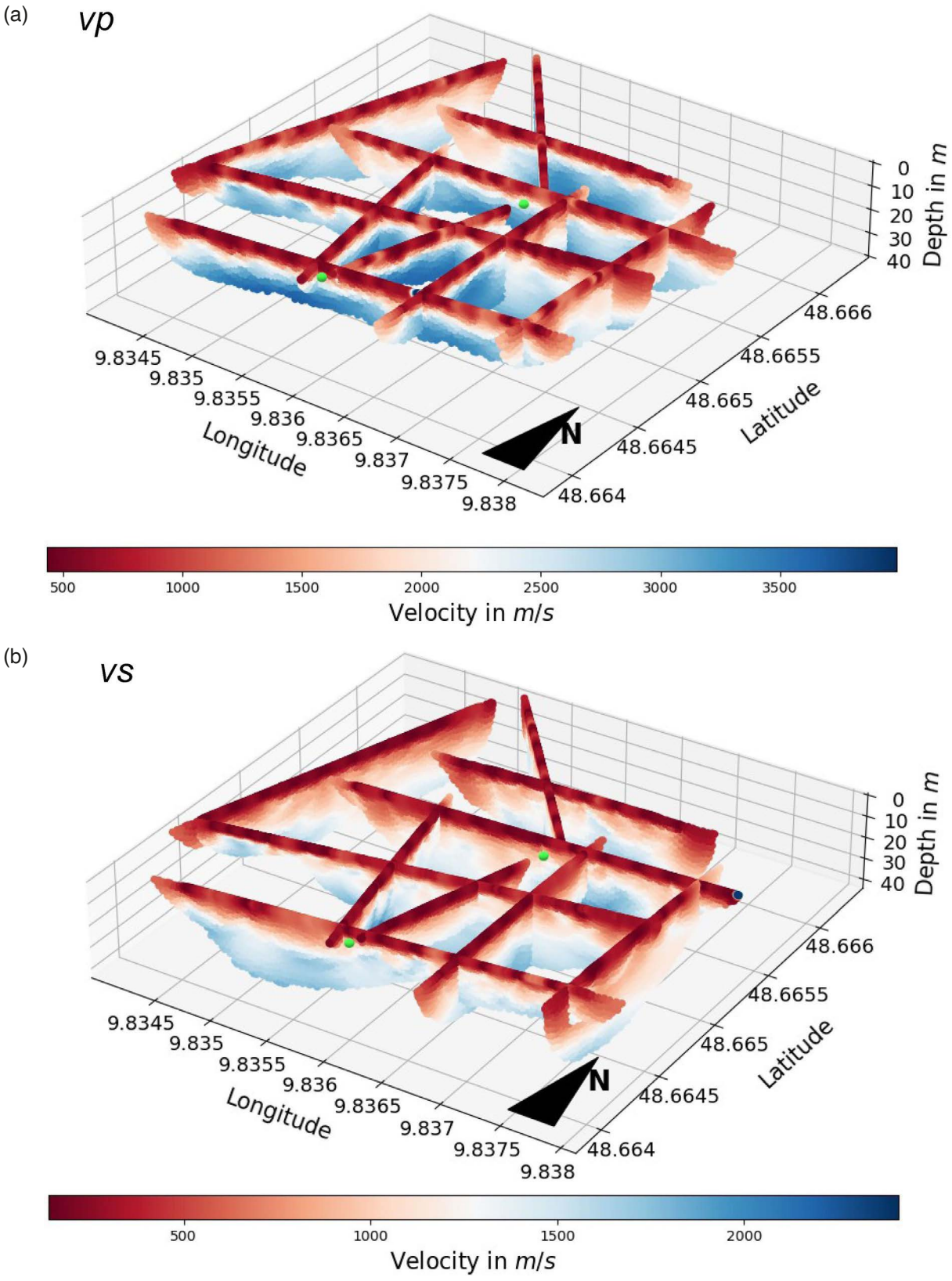

Figure 8. Fence diagrams with final seismic velocity models for WINSENT from cross-sections in Fig. 7, ((a) *vp*; (b) *vs*). Green dots are the locations of the two wind turbines. The lateral extent is ca. 300 m × 300 m, for location see Fig. 1.

range of about 3,100 m/s and *vs* reaches ca. 1.600 m/s. The shear wave velocity structure is more variable along the lines than the compressional wave velocity structure. This may be due to shallow karst cavities which are filled with clay (Fig. 2, right) and soil.

The ray coverage allows us to image the seismic velocities to 20-30 m depth, depending on the recording distance. Below 10 m depth *vp* is mostly above 3,000 m/s and *vs* exceeds 1,600 m/s. Lateral variation of *vp* and *vs* is low as expected from the horizonal layering of the limestone banks (Fig. 2). Clear deep-reaching (>2 m) karst cavities are not obvious, possibly they are below the nominal resolution of 6 m (cell width). However, low *vs* anomalies are found at 60-70 m distance at line P2 or 90-110 m distance along P9 (Fig. 7). A lateral *vs* contrast of ca. 500 m/s at 120 m distance at P3 is the clearest lateral feature. This anomaly is not characterized by a change in *vp* – hence a change in *vp*/*vs* may indicate a change a stiffness or fluid content. Low *vp* and *vs* are retrieved long line P6 in the east of the study area.

A velocity increase with depth of surface waves (1.2-8.33 Hz) was observed just 1-2 km to the south at the wind farm Tegelberg which has a nearly identical subsurface (Gaßner et al., 2023). The surface waves with the highest analyzed frequency (8.33 Hz) and with a wavelength of ca. 130 m (penetration depth ca. 50 m) have velocities of 1070 m/s (mean) within a range of 510-2140 m/s. This corresponds to *vs* of ca. 960 m/s (surface wave velocity is ca. 0.9 *vs*) and lower than our model results (1,600 m/s).

Fence diagrams are plotted in Fig. 8 to better visualize the 3-D character of the *vp* and *vs* distribution at the wind energy test site WINSENT. The crossing velocity models mostly fit very well for *vp* and *vs*. An exception is the intersection between lines P1 and P5; here both, *vp* and *vs* are lower below P1 compared to P5 (Fig. 8, for location see Fig. 1).

3.3 Comparison with borehole information

The seismic velocity models can be compared with borehole data. Two boreholes were drilled at each of the construction sites for the two wind turbines. These sites are in the middle of the lines P3 (BK1 and BK2 at the northern WT) and P4 (BK3 and BK4 at the southern WT) (Fig. 1). The boreholes BK1-BK4 reach depths between 10 m and 12 m and cores were extracted (Smoltczyk and Partner GmbH, 2019). The lithologies consist – from top downwards – of a soil cover (few centimeters thickness), silt and clay (up to 4 m thickness at BK02, karst cavity?) and the limestone top is at 0.1-4 m depth (Fig. 9). The direct comparison between the borehole lithologies and the *vp* and *vs* models in Fig. 9 indicate no clear correlation between these rock properties. The lithological boundaries of BK01, BK03 and BK04 do not coincide with a change in seismic velocity. Only at BK02, where there is a thicker layer with

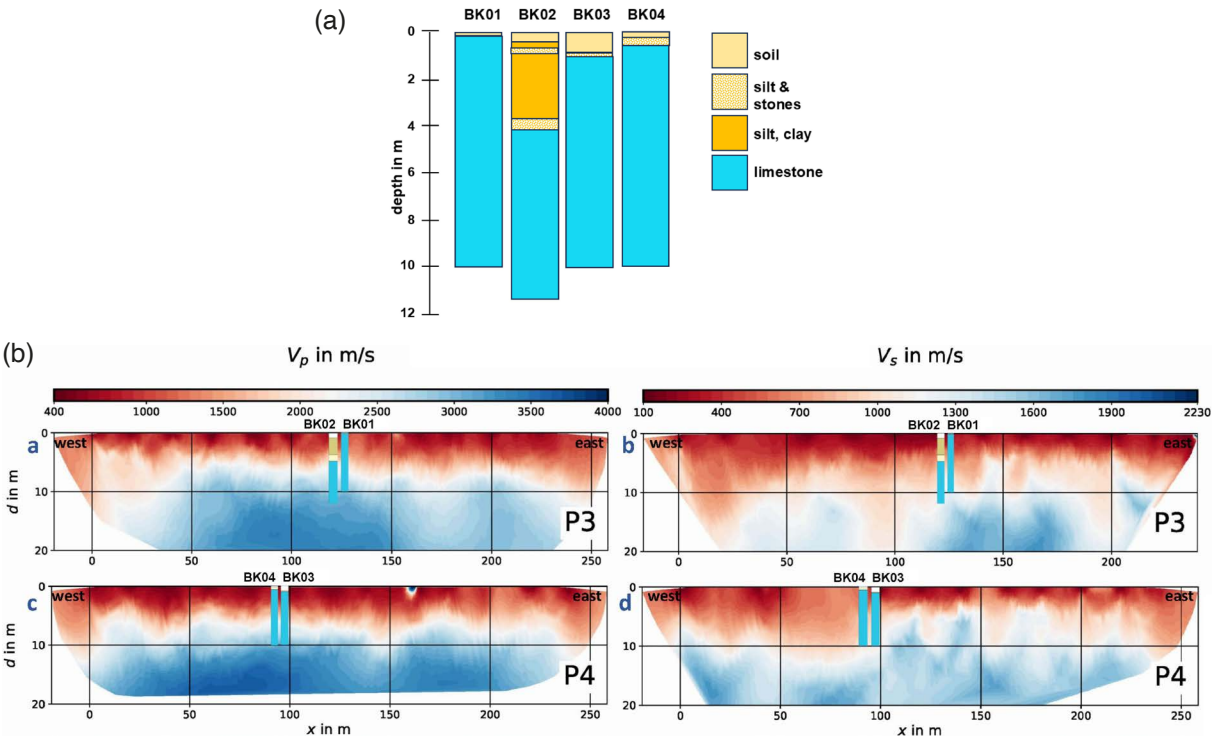

Figure 9. (a) Simplified lithological profiles for boreholes BK01-BK04 after Smoltczyk and Partner GmbH (2019) and (b) comparison of seismic models with borehole lithology.

silt, clay and (limestone) stones, a velocity contrast appears at the lithological boundary. The missing coincidences may be attributed to the resolution of the seismic inversion model (~6 m) with smearing along the ray paths and too coarse sensor distances in the field (2 m). The mostly lower *vp* and *vs* values compared to other studies (Table 1) may be due to deep reaching weathering effects which fractured the solid limestone banks and filled these with clay. Such a fractured and refilled medium, e.g. limestone and clay, and its effects on seismic velocity is described in Barton (2007). The actual velocity reduction compared to an intact, clay-free limestone depends strongly on the clay content or permeability of the limestone what is beyond the resolution of our data.

Table 1. Depth ranges (*d*) and seismic velocities of compressional (*vp*) and shear (*vs*) waves and their sources. The fourth column gives the average velocity measured at the wind energy test site WINSENT.

Lithology	*vp* in m/s	*vs* in m/s	Average in this study		Depth in m
			vp in m/s	*vs* in m/s	
Soil, weathering	100-500[a] 300-700[d] 400-1,200[i] 245-1,151[j]	70-150[g] 114-522[j]	500	160	0.05-0.2
Silt, clay	2,000-4,700[a] 500-1,500[d] 1,100-2,500[e] 1,800-2,400[f] 1,100-2,500[i]	1,400-2,600[a] 500-900[d] 230-360[g] 210-480[h]	1,700	800	0.05-4.0
Limestone	2,000-6,200[a] 3,390-5,790[b] 3,500-6,000[c] 4,300-5,800[d] 5,970-6,600[e] 4,890-6,370[f] 2,800-6,400[i]	1,800-3,800[a] 1,670-3,040[b] 2,000-3,300[c] 2,600-3,200[d] 2,880-3,030[e] 2,540-3,700[f]	<20 m depth: 3,100 >20 m depth: >3,000-4,000	1,600 1,600-2,200	0.05->20

(a) Knödel et al. (1997), (b) Mavko et al. (1998), (c) Mari (2019), (d) Styles (2022), (e) Dobrin and Savit (1988), (f) Hellwege (1982), (g) Karray and Lefebvre (2009), (h) Zhu et al. (2008), (i) Barton (2007), (j) Uyanik (2019) (see References).

4. Conclusions

At the wind energy test site WINSENT, a seismic field experiment was successfully accomplished. Although an explosive source could not be used, eight stacked hammer blows were enough to record P- and S-wave with a very good SNR for up to 200 m distance. This good wave propagation is attributed to the thin soil layer and the stiff limestone underneath which does not cause much damping.

The *vp* and *vs* models do not vary laterally much in two dimensions (Fig. 7) and three dimensions (Fig. 8) within about 300 m across WINSENT. In vertical direction there is an increase of *vp* and *vs* with depth. This relatively simple structure is helpful for synthetic modelling the wave propagation of ground motion emissions from the wind turbines. Once a source function is determined which represents the soil-structure interaction of the wind turbines with the ground, only a depth-dependent elastic model needs to be implemented for wavefield modelling.

In the limestone layer(s) the *vp* and *vs* values in the inversion model (Figs. 7-9) are low compared to other studies (Table 1). This difference can be explained with weathering effects and karstification what allows soil and clay to penetrate downwards into the rock body along fractures or joints. Thereby the stiffness of the in situ rock body is reduced compared to a solid limestone body (Barton, 2007). For numerical wave propagation modelling this reduced *vp* and *vs* needs to be accounted for, although the small-scale material variations across clayed-filled cavities may not resolved for model dimensions of several hundred (or even thousand) meters.

The low damping of the hammer blow signals in the limestone could be a hint for similar low damping of WT emissions along longer distances. WT turbine emissions are mostly seismic surface waves (Neuffer et al., 2021; Gaßner et al., 2023). These waves have frequencies as low as ca. 0.3 Hz (fundamental frequency of the tower) and 10 Hz signals are observed in seismic records at distances of several kilometers (Stammler and Ceranna, 2016). For a frequency range of 0.5-5 Hz and an average shear wave velocity of 2000 m/s at some 100 m depth, a surface wave has a wavelength of about 360-3,600 m (a factor of 0.9 is applied to convert *vs* to surface wave velocity). This wavelength estimation means that within 3.6-36 km distance from a WT, corresponding to about ten wavelengths, anelastic damping would be low compared to the geometric spreading effect of the WT ground motion emissions (see also Gaßner et al., 2023).

Local, sometimes small-scale measurements of geotechnical parameters are essential for understanding effects of soil-structure interaction and resulting emissions, e.g. ground motions. Values from existing literature (Table 1) may be good approximations, however, upscaling of laboratory values (often high frequency waves and intact rock samples) and transfer to natural in situ rock bodies can fail. Therefore, field experiments should be conducted whenever and wherever possible at sites with critical infrastructure to estimate a possible impact of ground motions.

Our petrophysical results will be compared with the geotechnical measurements as soon as these are available. In this way, the derived elastic moduli can be compared between both methods and then they can be chosen for a final underground model around the WT foundation. Such an underground model together with the 3-D *vp* and *vs* structures are the basis for inverting a source model for the movement of the WT foundation based on the waveforms of the emitted ground motions (Cesca et al., 2010). The source model can later be applied to other wind turbines and regions where a prediction of ground motions is wanted, e.g. near high-sensitive infrastructure (Diaferia et al., 2024).

Data availability statement. The seismic data is available by request from J. Ritter (joachim.ritter@kit.edu).

Acknowledgements. We thank Dario Eickhoff, Philipp Fesseler, Marius Grimmhausen and Leon Merkel for help and advice during the fieldwork. A. Rettenmeier (ZSW Stuttgart) is thanked for assisting this project and the permitting. Smoltczyk and Partner GmbH kindly provided borehole data. Two reviewers provided helpful comments to improve the manuscript. *Refrapy* (Guedes et al., 2022) was used for data analysis. Fence diagrams were built with pyproj, https://pyproj4.github.io/pyproj/stable/. We acknowledge financial support by the German Federal Ministry for Economic Affairs and Climate Action, project WINSENTvalid, no. 03EE2028B.

References

Barton, N. (2007). Rock quality, seismic velocity, attenuation, and anisotropy, Taylor and Francis, Balkema, Leiden, 729, ISBN:0-415-39441-4.

Cesca, S., S. Heimann, K. Stammler and T. Dahm (2010). Automated procedure for point and kinematic source inversion at regional distances, J. Geophys. Res., 115, B06304, doi:10.1029/2009JB006450.

Diaferia, G., C. Giunchi, M. Olivieri, I. Molinari et al. (2024). Seismic noise characterisation for the Buddusò – Ala dei Sardi wind park (Sardinia, Italy) and its impact on the Einstein Telescope candidate site, EGUsphere, preprint, doi:10.5194/egusphere-2024-3600.

Dobrin, M. B. and C. H. Savit (1988). Introduction to Geophysical Prospecting, 4th ed., McGraw-Hill, Singapore, 867, ISBN:0-07-017196-3.

Gaßner, L., M. A. Gärtner and J. Ritter (2023). Simulation of ground motion emissions from wind turbines in low mountain ranges: implications for amplitude decay prediction, J. Seismol., 27, 933-952, doi:10.1007/s10950-023-10172-6.

GEOMETRICS (2024). https://www.geometrics.com/product/geode-exploration-seismograph/, last access 26 Dec. 2024.

GEOSYM (2024). Description of Seismic Impulse Source Sissy, https://www.geosym.de/en/systems#anker_sissy_en, last access 26 Dec. 2024.

Guedes, V. J. C. B., S. T. R. Maciel and M. P. Rocha (2022). Refrapy: A Python program for seismic refraction data analysis, Comput. Geosci., 159, 105020, doi:10.1016/j.cageo.2021.105020.

Hellwege, K. H. (1982). Landolt-Börnstein, Numerical data and relationships in science and technology, new series, 1, Physical Properties of Rocks, subvolume b, Springer-Verlag, Berlin, ISBN:3-540-11070-4.

International Energy Agency (2024). Renewables 2023 – analysis and forecast to 2028, 141, https://www.iea.org/reports/renewables-2023.

Karray, M. and G. Lefebvre (2009). Techniques for mode separation in Rayleigh wave testing, Soil Dyn. Earthq. Eng, 29, 4, 607-619, doi:10.1016/j.soildyn.2008.07.005.

Knödel, K., H. Krummel and G. Lange (1997). Handbuch zur Erkundung des Untergrundes von Deponien und Altlasten, 3, Geophysik, Springer-Verlag, Berlin, 1063, ISBN:3-540-59462-0.

Lerbs, N., T. Zieger, J. Ritter and M. Korn (2020). Wind turbine induced seismic signals: the large-scale SMARTIE 1 experiment and a concept to define protection radii for recording stations, Near Surf. Geophys., 18, 467-482, doi:10.1002/nsg.12109.

Limberger, F., G. Rümpker, M. Lindenfeld and H. Deckert (2022). Development of a numerical modelling method to predict the seismic signals generated by wind farms, Sci. Rep., 12, 15516, doi:10.1038/s41598-022-19799-w.

Mari, J. L. (2019). Seismic Imaging: a practical approach, EDP Sciences, doi:10.1051/978-2-7598-2351-2.c003.

Mavko, G., T. Mukerji and J. Dvorkin (1998). The rock physics handbook, Cambridge University Press, Cambridge, 329, ISBN:0-521-62068-6.

Nagel, S., T. Zieger, B. Luhmann, P. Knödel et al. (2021). Ground motions induced by wind turbines, Civil Eng. Design, 3, 73-86, doi:10.1002/cend.202100015.

Neuffer, T., S. Kremers, P. Meckbach and M. Mistler (2021). Characterization of the seismic wave field radiated by a wind turbine, J. Seismol., 25, 825-844, doi:10.1007/s10950-021-10003-6.

Peña, C., S. Gehring, P. Fesseler, H. H. Stutz et al. (2025). Integrierte geotechnische Untersuchung zur Anregung und Ausbreitung von Bodenbewegungen an Forschungswindenergieanlagen, Baudynamik, 2447, 325-336, VDI Verlag, doi:10.51202/9783181024478-325.

Regierungspräsidium Freiburg, Landesamt für Geologie, Rohstoffe und Bergbau Hrsg (2021). LGRB-Kartenviewer – Layer GeoLa-GK50: Geologische Einheiten (Flächen), https://maps.lgrb-bw.de/.

Saccorotti, G., D. Piccinini, L. Cauchie and I. Fiori (2011). Seismic noise by wind farms: a case study from the Virgo Gravitational Wave Observatory, Italy, Bull. Seismol. Soc. Am., 101, 568-578, doi:10.1785/0120100203.

Smoltczyk and Partner GmbH (2019). Geotechnischer Bericht, 19-019 Stötten, Donzdorf-Immenreute, Windenergieanlage WindForS, date 17/06/19, Stuttgart, 56, in German.

Stammler, K. and L. Ceranna (2016). Influence of wind turbines on seismic records of the Gräfenberg array, Seismol. Res. Lett., 87, 5, 1075-1081, doi:10.1785/0220160049.

Starreveld, W. S. (2023). Safety impact of wind turbines in the vicinity of aerodromes and air routes, SIG Aviation, Kraainem, Belgium, EASA.2019.CEI.14.EC021.

Styles, P. (2022). Environmental Geophysics – everything you ever wanted (needed!) to know but were afraid to ask! EAGE Publications bv, Houten, 220, ISBN:978-90-73834-33-0, doi:10.3997/9789073834330.

Uyanık, O. (2019). Estimation of the porosity of clay soils using seismic P- and S-wave velocities, J. Appl. Geophys., 170, 103832, doi:10.1016/j.jappgeo.2019.103832.

Zhu, F., K. R. Peaker and A. Shaheen (2008). Field measurement of shear wave velocity of soils, GeoEdmonton'08, 986-991, last access 31 Dec. 2024, Microsoft Word - GEO08Paper473.doc.

***CORRESPONDING AUTHOR: Joachim RITTER**,
Karlsruhe Institute of Technology, Geophysical Institute, Karlsruhe, Germany
e-mail: joachim.ritter@kit.edu